Circuital Model Validation for S-Shaped Organic Solar Cells by Means of Impedance Spectroscopy

B. Romero, G. del Pozo, B. Arredondo, J. P. Reinhardt, M. Sessler, and U. Würfel

***Abstract*—Organic solar cells (OSCs) based on Poly[N-9′-heptadecanyl-2,7-carbazole-alt-5, 5-(4′, 7′-di-2-thienyl-2′,1′,3′-benzothiadiazole)] (PCDTBT):1-(3-methoxycarbonyl)-propyl-1-1-phenyl-(6,6) C61 (PCBM) have been electrically dc and ac characterized. Device structure is ITO/Poly(3,4-ethylenedioxy-wthiophene)-poly(4-styrene sulfonate) (PEDOT:PSS)/PCDTBT: PCBM/C_{60}MA/Al. Devices show the so-called S-shaped current–voltage curve that has been modeled with a circuit including two diodes in forward and reverse bias. Impedance measurements show one semicircle at low bias ($V < 0.4$ V) and two semicircles at $V \geq 0.4$ V. Results reveal that the high-frequency semicircle is associated with the forward diode-like behavior of the dc circuit, while the low-frequency semicircle is associated with the reverse diode that causes the S-shape. The analytical solution of the dc two-diode circuital model has been fitted to the experimental *I–V,* and dc circuital parameters have been obtained. The ac equivalent circuit was derived from the dc circuit, and small-signal parameters have been calculated from the fits to the experimental Cole–Cole.**

***Index Terms*—Circuit modeling, impedance spectroscopy (IS), organic solar cells (OSCs), S-shape.**

I. Introduction

OVER the past few years, organic solar cells (OSCs) have become very popular due to the rapid evolution of this technology based on both small organic molecules and polymeric materials [1], [2]. Organic devices are flexible, thin, and lightweight. Moreover, fabrication costs are much lower than those of silicon-based devices, allowing large area scalability without a significant increase of the expenses [3], [4]. State-of-the-art efficiencies in these devices have recently exceeded 10% [5].

However, OSCs frequently show the so-called S-shape, a curvature change in the current–voltage (*I–V*) characteristic [6]–[9]. This S-shape drastically reduces fill factor and, therefore, device efficiency. The physical origin of the S-shape is still a matter of controversy. The most extended hypothesis points out that S-shape is caused by an accumulation of carriers inside the device, which results in a change of the electric field distribution [10], or in other words, S-shape is related to poor electron extraction layers [11], [12]. S-shape has been found in devices with different structures, both direct and inverted, and in devices with different active layer materials, such as the standard poly(3-hexylthiophene) (P3HT): 1-(3-methoxycarbonyl)-propyl-1-1-phenyl-(6,6) C61 ($PC_{60}BM$), and in poly(benzo[12-*b*:4,5-*b*′]dithiophene-thieno [3,4-*c*]pyrrole-4,6-dione) (PBDTTPD): [6,6]-phenyl-C71-butyric acid methyl ester ($PC_{71}BM$) [13]. Some authors have focused their efforts in removing S-shape by means of thermal annealing or UV-light illumination [14].

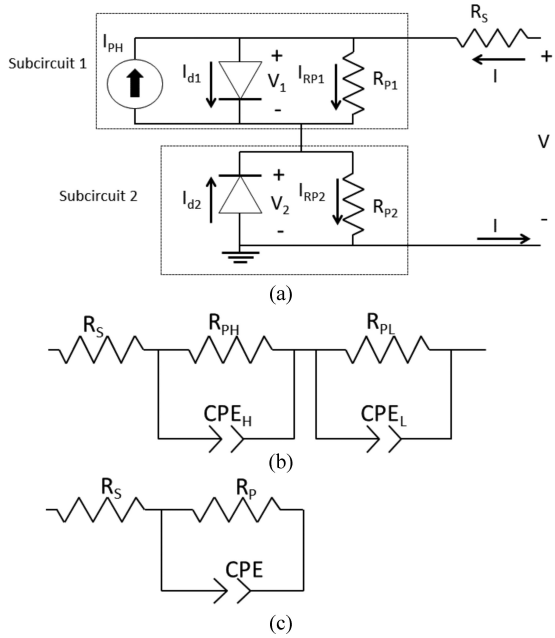

Fig. 1. (a) Circuital models to simulate *I–V* characteristic (dc). (b), (c) Impedance spectra (ac).

On the other hand, circuit modeling is a valuable tool to understand the electrical behavior of organic devices. Some authors have proposed different dc models for S-shaped OSCs, since the standard traditional circuit, based on a single diode in parallel with a constant current source and parasitic resistances, is not able to simulate the curvature change in the *I–V* curve. Araujo *et al.* proposed a simple circuital model that includes one extra diode to simulate this curvature change, taking into account the semiinsulating behavior of the electrodes [15] [see Fig. 1(a)]. This circuit is the series combination of two subcircuits: the standard one that includes the forward diode (subcircuit 1), and the one including the reverse diode (subcircuit 2). More complicated circuits including two extra diodes can also be found in the literature [16].

Manuscript received September 15, 2014; revised October 2, 2014; accepted October 8, 2014. Date of publication November 5, 2014; date of current version December 18, 2014. This work was supported by Comunidad Autónoma de Madrid and Universidad Rey Juan Carlos under Project S2009/ESP-1781.

B. Romero, G. del Pozo, and B. Arredondo are with the Electronic Technology Department, University Rey Juan Carlos, 28933 Madrid, Spain (e-mail: beatriz.romero@urjc.es; gonzalo.delpozo@urjc.es; belen.arredondo@urjc.es).

J. P. Reinhardt is with the Freiburg Materials Research Center, University of Freiburg, 79104 Freiburg, Germany (e-mail: jens.reinhardt@ise.fraunhofer.de).

M. Sessler and U. Würfel are with the Freiburg Materials Research Center, University of Freiburg, 79104 Freiburg, Germany, and also with the Fraunhofer Institute for Solar Energy Systems ISE, 79110 Freiburg, Germany (e-mail: martin.sessler@ise.fraunhofer.de; uli.wuerfel@ise.fraunhofer.de).

Digital Object Identifier 10.1109/JPHOTOV.2014.2362978

Concerning the ac regime, several authors have proposed different small-signal models to simulate OSC impedance spectroscopy (IS) measurements: 1) the simple *RC* circuit [17]–[20]; 2) the R-CPE circuit [see Fig. 1(c)] [19], [21]; 3) the transmission line circuit proposed by Belmonte [19], [22]; and 4) the circuit proposed by Ecker *et al.* [9].

To our knowledge, no work has so far related dc and ac behavior for OSCs showing S-shape in *I–V* characteristics. In this paper, we have measured dc and ac electrical characteristics of an OSC with the S-shaped *I–V* curve based on poly(N-9′-heptadecanyl-2,7-carbazole-alt-5,5-(4′,7′-di-2-thienyl-2′,1′, 3′-benzothiadiazole) (PCDTBT) blended with $PC_{71}BM$. Device structure is ITO/PEDOT:PSS/PCDTBT:$PC_{71}BM$/$C_{60}MA$/Al. We have used the analytical solution given in [23] of the two-diode dc circuit model shown in Fig. 1(a) to fit the S-shaped *I–V* curve. We have derived the small-signal equivalent circuit using fundamental electronic rules, that is setting dc current source to zero and substituting forward and reverse diodes by nonideal parallel *RC* circuits [see Fig. 1(b)]. It is straightforward that for both subcircuits, the parallel resistance in ac equals $\mathrm{R_d}//\mathrm{R_P}$ in dc, where $\mathrm{R_d}$ is the dynamical resistance of the corresponding diode and $\mathrm{R_p}$ is the parallel resistance. The equivalent small-signal circuit has been fitted to IS measurements, and the resulting small-signal parameters at different bias (from 0 to 0.8 V) have been compared with those obtained from the dc fit. A good agreement was found between ac and dc parameters, validating the model.

II. Fabrication and Characterization

Patterned indium tin oxide (ITO) glass substrates were cleaned in ultrasonic baths following the typical organic material cleaning process. Substrates were exposed for 20 min to ozone irradiation. A hole transport layer of AI4083 PEDOT:PSS was spin-coated and subsequently annealed in an oven for 10 min at 130 °C to obtain a ∼40-nm-thick layer. The active layer was spin-coated from solution containing a PCDTBT:$PC_{71}BM$ blend with 7-mg PCDTBT and 28 mg of $PC_{71}BM$ in 1 ml ortho-dichlorobenzene. The solution was stirred for several hours and spin-coated at 720 r/min to obtain an 80-nm-thick active layer. Samples were baked on a hot plate at 150 °C for 15 min. $C_{60}MA$, which is a solution-processable electron-selective layer first used by Jen *et al.* [24], [25], was deposited by spin coating at 3000 r/min. Finally, the Al electron contact was thermally evaporated on top of the device through a shadow mask in an atmosphere of 10^{-6} torr. All processes were carried out in a glove box in an inert atmosphere with levels of H_20 and $O_2 < 0.1$ ppm. Device active area is 9 mm^2.

The *I–V* curves were measured using a Keithley 2400 Sourcemeter and a Steuernagel SolarCellTest 575 sun simulator. Impedance spectra were recorded using an IM6 Electrochemical Workstation at Zahner-elektrik. Samples were measured inside a flow cell, where a constant nitrogen flow was set in order to avoid degradation. A halogen lamp was used for illumination. Impedance spectra were recorded by applying a small voltage perturbation (20 $\mathrm{mV_{rms}}$) at frequencies from 1 to 1 Hz at different dc voltages.

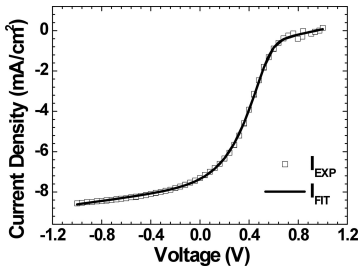

Fig. 2. Experimental (symbols) and fit (solid line) *I–V* curve of a PCDTBT:$PC_{71}BM$-based device.

TABLE I
CIRCUITAL PARAMETERS OBTAINED FROM THE *I–V* FIT

I_{01} (mA)	I_{02} (mA)	n_1	n_2	R_{P1} (kΩ)	R_{P2} (kΩ)
5.7 10^{-3}	2.5 10^{-5}	7.3	1.5	16.4	4.9

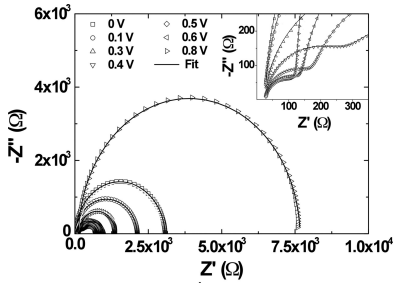

Fig. 3. IS measurements at different bias voltages, from 0 up to 0.8 V (symbols) and fit (solid lines). Inset shows a zoom for the high-frequency range.

III. Results and Discussion

A. Direct Current

Fig. 2 shows the *I–V* curve, experimental data (symbols) and fit (solid line) using the circuit of Fig. 1(a). This circuit includes a counter diode responsible for the S-shape, which is associated with poor electron extraction layers, in our case to the $C_{60}MA$/Al cathode. Even though including a C60MA layer usually improves the cell electrical performance as demonstrated in [25], in this case, the degradation of this layer may be responsible for the S-shape. Nevertheless, no matter what the physical origin of this feature is, the scope of this paper is to analyze it by means of circuital modeling.

Experimental data of Fig. 2 were fitted using the circuit analytical solution derived in [23].

Circuital parameters obtained from the fit are shown in Table I, where I_{01} and I_{02} are the inverse saturation currents, n_1 and n_2 are ideality factors, R_{P1} and R_{P2} are parallel resistances of forward diode 1 and reverse diode 2, respectively, and R_s is the series resistance with value 30 Ω.

B. Alternating Current

Fig. 3 shows IS data (symbols) of the device at different bias voltages from 0 to 0.8 V under illumination. Inset shows a zoom

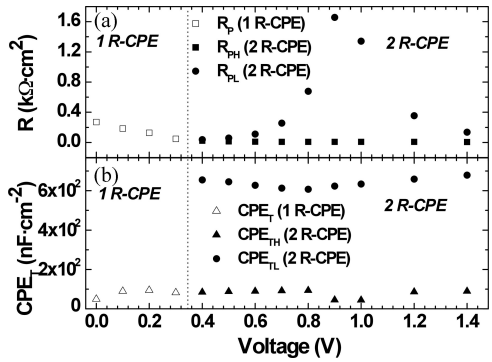

Fig. 4. Resistance (a) and capacitance (CPE_T) (b) versus bias voltage. Parameters are extracted from the fit using models of Fig. 1(b) and (c) for spectra showing two and one semicircles, respectively.

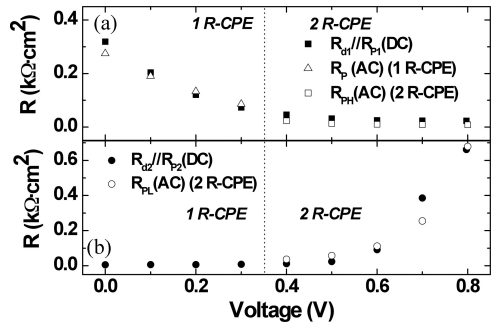

Fig. 5. Resistance versus voltage associated with the high-frequency range (a) and low-frequency range (b) using models 1R-CPE and 2R-CPE. Resistance obtained from the dc fit is shown for the sake of comparison.

in the high-frequency range. The IS data show one semicircle for $\mathrm{V} < 0.4$ V and two depressed semicircles for $\mathrm{V} \geq 0.4$ V, that have been fitted with circuits of Fig. 1(c) and (b), respectively. Solid lines in Fig. 3 show the fits. It is worth noticing that the circuits of Fig. 1(a) and (b) represent the same circuital model in its dc and ac version, respectively. As mentioned before, small-signal circuit of Fig. 1(b) has been derived from its corresponding dc circuit [see Fig. 1(a)] substituting each diode by a resistance in parallel with a constant phase element (CPE). A CPE resembles a nonideal capacitor that takes into account nonhomogeneities, such as porosities, roughness, and surface states with $Z_{\mathrm{CPE}} = \frac{1}{(\mathrm{CPE}_T)(j\omega)^{(\mathrm{CPE}_P)}}$, where CPE_T and CPE_P are impedance parameters [26]. Whenever CPE_P is close to 1, CPE_T can be approximated to a capacitor. $\mathrm{R_S}$ models metallic contacts, wires, etc., and $\mathrm{R_P}$ accounts for the parallel of the diode dynamical resistance and shunt resistance.

Taking into account the voltage dependence of the Cole–Cole shape, the fits were performed using the circuit of Fig. 1(c) for voltages < 0.4 V (one semicircle) and the circuit of Fig. 1(b) for voltages ≥ 0.4 V (two semicircles). The fitting parameters are $\mathrm{R_S}$, $\mathrm{R_P}$, CPE_P, and CPE_T for single semicircle spectra, and $\mathrm{R_S}$, R_{PL}, $\mathrm{CPE_{PL}}$, $\mathrm{CPE_{TL}}$, R_{PH}, $\mathrm{CPE_{PH}}$, and $\mathrm{CPE_{TH}}$ for spectra showing two semicircles. Subindex L stands for "low frequency," and subindex H stands for "high frequency." Fitting parameters CPE_P, $\mathrm{CPE_{PL}}$, and $\mathrm{CPE_{PH}}$ are > 0.9 in all cases, meaning that the CPE elements can be considered as ideal capacitors with CPE_T being the capacitance value.

Fig. 4 shows the parameters resulting from the fits. Fig. 4(a) shows the resistance $\mathrm{R_P}$ associated with the circuit of Fig. 1(c), and resistances R_{PH} and R_{PL} corresponding to the circuit of Fig. 1(b). Fig. 4(b) displays CPE_T parameters, CPE_T related to the circuit of Fig. 1(c), and $\mathrm{CPE_{TH}}$ and $\mathrm{CPE_{TL}}$ associated with the circuit of Fig. 1(b). In view of the smooth matching trend between CPE_T and $\mathrm{CPE_{TH}}$, and $\mathrm{R_P}$ and R_{PH}, we conclude that the recombination mechanism associated with the high-frequency semicircle for $\mathrm{V} \geq 0.4$ V is the continuation of the recombination mechanism of the single semicircle observed for $\mathrm{V} < 0.4$ V. Moreover, since no S-shape is observed for $\mathrm{V} < 0.4$ V, we conclude that the high-frequency recombination semicircle is linked to the forward diode in Fig. 1(a). Reverse diode in Fig. 1(a), responsible for S-shape at $\mathrm{V} > 0.4$ V, is linked to the low-frequency semicircle observed in IS measurements at $\mathrm{V} > 0.4$ V. This is in good agreement with results obtained by other authors [12], and confirms that the kink is probably due to a slow-charge transfer process at the electron contact, that is modeled by the reverse diode. In this case, S-shape cannot be attributed to imbalanced charge mobility in the PCDTBT:$\mathrm{PC_{71}BM}$ [9], since there are previous works using this photoactive material with no evidence of kink [27]. The large capacitance associated with the low-frequency semicircle $\mathrm{CPE_{TL}}$ is due to charge accumulation in the cathode. The capacitance related to the forward diode $\mathrm{CPE_{TH}}$, at low bias is associated with the geometrical capacitance. As bias is increased, carriers are injected, and $\mathrm{CPE_{TH}}$ begins to be dominated by chemical capacitance.

Fig. 5 shows a comparison between parameters extracted from the fit to dc and ac circuits. Assuming that the forward diode is associated with the high-frequency semicircle and the reverse diode to the low frequency one, it follows that the ac resistances R_{PH} and R_{PL} are related to the parallel combination of $\mathrm{R_{P1}//R_{d1}}$ and $\mathrm{R_{P2}//R_{d2}}$, respectively. Note that $\mathrm{R_{d1}}$ and $\mathrm{R_{d2}}$ are the dynamical resistances of forward and reverse diodes, respectively, with $R_d = \frac{nV_T}{I_0 \exp\left(\frac{V}{nV_T}\right)}$. As can be observed, a good agreement has been obtained when comparing R_{PH} with $\mathrm{R_{P1}//R_{d1}}$, and R_{PL} with $\mathrm{R_{P2}//R_{d2}}$.. A close analysis of the behavior of individual voltage drops in each diode reveals that as the overall voltage increases, $\mathrm{V_1}(= \mathrm{V_{d1}})$ increases, and $\mathrm{V_2}(= -\mathrm{V_{d2}})$ also increases, thus decreasing $\mathrm{V_{d2}}$. This means that $\mathrm{R_{d1}}$ decreases and $\mathrm{R_{d2}}$ increases with total voltage. This is reflected in the trends of Fig. 5.

IV. Conclusion

In summary, we have analyzed OSCs presenting S-shaped *I–V* characteristics using IS. We conclude that the recombination mechanism related to the high-frequency semicircle in the Cole–Cole diagram for $\mathrm{V} \geq 0.4$ V is modeled by the forward diode in the circuit of Fig. 1(a). This semicircle is the continuation of the single semicircle observed at $\mathrm{V} < 0.4$ V. On the other hand, the low-frequency semicircle in the impedance spectra for $\mathrm{V} \geq 0.4$ V is associated with the reverse diode causing the

S-shape. Finally, ac and dc parameters extracted from the fits are in good agreement, validating the dc circuit used to model S-shaped *I–V* curves of OSCs.

ACKNOWLEDGMENT

The authors would like to acknowledge R. Vergaz for fruitful discussions on impedance spectroscopy analysis.

REFERENCES

[1] C. J. Brabec, N. S. Sariciftci, and J. C. Hummelen, "Plastic solar cells," *Adv. Funct. Mater.*, vol. 11, pp. 15–26, 2001.

[2] C. J. Brabec, S. Gowrisanker, J. J. M. Halls, D. Laird, D. S. J. Jia, and S. P. Williams, "Polymer-fullerene bulk-heterojunction solar cells," *Adv. Mater.*, vol. 22, pp. 3839–3856, 2010.

[3] H. J. Park, M. G. Kang, S. H. Ahn, and L. J. Guo, "A facile route to polymer solar cells with optimum morphology readily applicable to a roll-to-roll process without sacrificing high device performance," *Adv. Mater.*, vol. 22, pp. 247–253, 2010.

[4] F. C. Krebs, "Fabrication and processing of polymer solar cells: A review of printing and coating techniques," *Sol. Energy Mater. Sol. Cells*, vol. 93, pp. 394–412, 2009.

[5] N. S. Scharber and N. S. Sariciftci, "Efficiency of bulk-heterojunction organic solar cells," *Prog. Polymer Sci.*, vol. 38, pp. 1929–1940, 2013.

[6] A. Wagenpfahl, D. Rauh, C. Binder, C. Deibel, and V. Dyakonov, "S-shaped current-voltage characteristics of organic solar devices," *Phys. Rev. B*, vol. 82, pp. 115306-1–115306-9, 2010.

[7] A. Kumar, S. Sista, Y. Yang, "Dipole induced anomalous S-shape I-V curves in polymer solar cells," *J. Appl. Phys.*, vol. 105 pp. 094512-1–094512-6, 2012.

[8] B. Ecker, H. J. Egelhaaf, R. Steim, J. Parisi, and E. von Hauff, "Understanding S-shaped current-voltage characteristics in organic solar cells containing a TiO_x interlayer with impedance spectroscopy and equivalent circuit analysis," *J. Phys. Chem. C*, vol. 116, pp. 16333–16337, 2012.

[9] W. Tress, A. Petrich, M. Hummert, M. Hein, and K. Leo, "Imbalanced mobilities causing S-shaped *I–V* curves in planar heterojunction organic solar cells," *Appl. Phys. Lett*, vol. 98, pp. 063301-1–063301-3, 2011.

[10] J. C. Wang, X. C. Ren, S. Q. Shi, C. W. Leung, and P. K. L. Chan, "Charge accumulation induced S-shape *J–V* curves in bilayer heterojunction organic solar cells," *Org. Electron.*, vol. 12, pp. 880–885, 2011.

[11] B. Qi and J. Wang, "Fill factor in organic solar cells," *Phys. Chem. Chem. Phys.*, vol. 15, pp. 8972–8982, 2013.

[12] M. Glatthaar, M. Riede, N. Keegan, K. Sylverster-Hvid, B. Zimmermann, M. Niggemann, A. Hinsch, and A. Gombert, "Efficiency limiting factors of organic bulk heterojunction solar cells identified by electrical impedance spectroscopy," *Sol. Energy Mater. Sol. Cells*, vol. 91, pp. 390–393, 2007.

[13] W. R. Mateker, J. D. Douglas, C. Cabanetos, I. T. Sachs-Quintana, J. A. Bartelt, E. T. Hoke, A. E. Labban, P. M. Beaujuge, J. M. J. Fréchet, and M. D. McGehee, "Improving the long-term stability of PBDTTPD polymer solar cells through material purification aimed at removing organic impurities," *Energy Environ. Sci.*, vol. 6, pp. 2529–2537, 2013.

[14] S. Chambon, E. Destouesse, B. Pavageau, L. Hirsch, and G. Wantz, "Towards an understanding of light activation processes in titanium oxide based inverted organic solar cells," *J. Appl. Phys.*, vol. 112, pp. 094503-1–094503-6, 2012.

[15] F. A. de Castro, J. Heier, F. Nüesch, and R. Hany, "Origin of the kink in current-density versus voltage curves and efficiency enhancement of polymer-C60 heterojunction solar cells," *IEEE J. Sel. Topics Quantum Electron*, vol. 16, no. 6, pp. 1690–1699, Feb. 2010.

[16] B. Mazhari, "An improved solar cell circuit model for organic solar cells," *Sol. Energy Mater. Sol. Cells*, vol. 90, pp. 1021–1033, 2006.

[17] P. Kavak, U. D. Menda, E. A. Parlak, O. Ozdemir, and K. Kutlu, "Excess current/capacitance observation on polymer-fullerene bulk heterojunction, studied through *I–V* and *C/G–V* measurements," *Sol. Energy Mater. Sol. Cells*, vol. 103, pp. 199–204, 2012.

[18] T. W Zeng, C. C Ho, Y. C. Tu, G. Y. Tu, L. Y. Wang, and W. F. Su, "Correlating interface heterostructure, charge recombination and device efficiency of poly(3-hexul thiophene)/TiOs nanorod solar cell," *Langmuir*, vol. 27, pp. 15255–15260, 2011.

[19] G. Perrier, R. de Bettignies, S. Berson, N. Lemaitre, and S. Guillerez, "Impedance spectrometry of standard and inverted P3HT:PCBM organic solar cells," *Sol. Energy Mater. Sol. Cells*, vol. 101, pp. 210–266, 2012.

[20] A. Guerrero, S. Loser, G. Garcia-Belmonte, C. J. Bruns, J. Smith, H. Miyauchi, S. I. Stupp, J. Bisquert, and T. J. Marks, "Solution-processed small molecule: fullerene bulk-heterojunction solar cells: Impedance spectroscopy deduced bulk and interfacial limits to fill-factors," *Phys. Chem. Chem. Phys.*, vol. 15, pp. 16456–16462, 2013.

[21] T. Kuwabara, C. Iwata, T. Yamaguchi, and K. Takahashi, "Mechanistic insights into UV-induced electron transfer from PCBM to titanium oxide in inverted type organic thin film solar cells using AC impedance spectroscopy," *Appl. Mater. Interfaces*, vol. 2, pp. 2254–2260, 2010.

[22] G. García-Belmonte, A. Guerrero, and J. Bisquert, "Elucidating operating modes of bulk-heterojunction solar cells from impedance spectroscopy analysis," *Phys. Chem. Lett.*, vol. 4, pp. 877–886, 2013.

[23] B. Romero, G. del Pozo, and B. Arredondo, "Exact analytical solution of a two diode circuit model for organic solar cells showing S-shape using lambert W-functions," *Sol. Energy*, vol. 86, pp. 3026–3029, 2012.

[24] K. M. O'Malley, C.-Z. Li, H.-L. Yip, and A. K.-Y. Jen, "Enhanced open-circuit voltage in high performance polymer/fullerene bulk-heterojunction solar cells by cathode modification with a C60 surfactant," *Adv. Energy Mater.*, vol. 2, pp. 82–86, 2012.

[25] C.-Z. Li, C.-C. Chueh, H.-L. Yip, K. M. O'Malley, W.-C. Chen, and A. K.-Y. Jen, "Effective interfacial layer to enhance efficiency of polymer solar cells via solution-processed fullerene-surfactants," *J. Mater. Chem.*, vol. 22, pp. 8574–8578, 2012.

[26] E. Barsoukov and J. R. MacDonald, *Impedance Spectroscopy. Theory, Experiment, and Applications*. New York, NY, USA: Wiley-Interscience, 2005.

[27] J. Reinhardt, M. Grein, C. Bühler, M. Schubert, and U. Würfel, "Identifying the impact of surface recombination at electrodes in organic solar cells by means of electroluminescence and modeling,"*Adv. Energy Mater.*, vol. 4, pp. 1400081-1–1400081-9, 2014.

Authors' photographs and biographies not available at the time of publication.